

**PROPERTIES OF GOLD NANOPARTICLES AND ITS CONJUGATION
WITH BIOMOLECULES FOR DIAGNOSTIC APPLICATION**

SITI RABIZAH BINTI MAKHSIN

UNIVERSITI SAINS MALAYSIA

2013

**PROPERTIES OF GOLD NANOPARTICLES AND ITS CONJUGATION
WITH BIOMOLECULES FOR DIAGNOSTIC APPLICATION**

By

SITI RABIZAH BINTI MAKHSIN

**Thesis submitted in fulfillment of the requirements
for the degree of
Master of Science**

FEBRUARY 2013

DECLARATION

I hereby declare that I have conducted, completed the research work and written the dissertation entitled “Properties of Gold Nanoparticles and its Conjugation with Biomolecules for Diagnostic Application”. I also declare that it has not been previously submitted for the award of any degree or diploma or other similar title of this for any other examining body or University.

Name of student: Siti Rabizah Binti Makhsin

Signature:

Date: 31 – 01 – 2013

Witness by

Supervisor: Assoc. Prof. Dr. Khairunisak Abdul Razak

Signature:

Date: 31 – 01 – 2013

ACKNOWLEDGEMENTS

First and foremost, I would like to extend my deepest gratitude to my supervisor Assoc. Prof. Dr. Khairunisak Abdul Razak for her continuous supervision, trust, guidance and support from the initial to the final stage of my research. I believe I am not able to finish my project without the help, patience and valuable advices from her. My special gratitude also goes to my co-supervisors; Prof. Rahmah Noordin and Assoc. Prof. Dr. Azlan Abdul Aziz for their insightful ideas and suggestions throughout this research work. All of them have guided me in a scientific way to conduct a research with their profound knowledge and research experience.

I wish to extend my gratitude to Universiti Sains Malaysia through Research University Postgraduate Research Grant Scheme (RUPRGS) and National Science Fellowship (NSF) from the Ministry Science, Technology and Innovation (MOSTI) for the financial support. I also would like to express my sincere gratitude to School of Materials & Mineral Resources Engineering and Nanobiotechnology Research & Innovation (NanoBRI), INFORMM, USM for their technical support. I also would like to thank all staffs especially Mrs Dyana Zakaria and Mr Masrul for their technical support and help during my laboratory work as well as their assistance in samples characterization. I am also greatly indebted to my beloved husband, Mr Mohamad Azizi Omar and family for their patience, pray and support. Their unconditional love motivates me to go through the hard time to complete my work. My special thanks to all my colleagues especially Ms Hajarul, Ms Syafinaz, Ms Hashimah, Ms Soo Ai, Mr Navanithan, Mr Adrian and others for their help, support and always share my laughs and tears together. Thank you.

TABLE OF CONTENTS

	Page
TITLE	i
DECLARATION	ii
ACKNOWLEDGEMENTS	iii
TABLE OF CONTENTS	iv
LIST OF TABLES	ix
LIST OF FIGURES	xi
LIST OF ABBREVIATIONS	xviii
LIST OF SYMBOLS	xx
LIST OF PUBLICATIONS	xxi
ABSTRAK	xxii
ABSTRACT	xxiii
CHAPTER 1: INTRODUCTION	1
1.1 Introduction	1
1.2 Research motivation	3
1.3 Objectives	5
1.4 Scope of the work	6
1.5 Dissertation structure	6
CHAPTER 2: LITERATURE REVIEW	8
2.1 Introduction of Nanobiotechnology	8
2.2 Gold Nanoparticles (AuNPs)	11
2.2.1 Structures of AuNPs	12

2.2.2 Lattice parameters of AuNPs	13
2.2.3 Thermal properties of AuNPs	15
2.2.4 Optical properties of AuNPs	17
2.2.5 Steric stabilization and electrostatic properties of AuNPs	20
2.2.6 Biological properties of AuNPs	22
2.3 Synthesis and fabrication of AuNPs	26
2.3.1 Physical reduction method	27
2.3.2 Photochemical reduction	29
2.3.3.1 X-Ray-irradiation	29
2.3.3.2 UV-irradiation	30
2.3.3 Sonochemical	31
2.3.4 Biological reduction	32
2.3.5 Microwave irradiation approach	34
2.3.6 Chemical reduction	35
2.3.6.1 Solvent evaporation method	37
2.3.6.2 Citrate reduction method	38
2.3.6.3 Seeding-growth method	39
2.4 Parameters of chemical reduction method	45
2.4.1 Types of reducing agent	45
2.4.2 Reaction temperature	49
2.4.3 Effect of pH	49
2.4.4 Volume of precursor (gold chloride)	52
2.5 Application of AuNPs	53
2.5.1 Biomedical field	54
2.5.2.1 Diagnostic: Immunochromatographic strip assay	55

2.5.2.2 Contrast agent: X-ray Computed Tomography (X-ray CT)	56
2.5.2.3 Photothermal therapy (PT)	57
2.5.2.4 Electrochemical immunosensor	59
2.6 AuNPs conjugated biomolecules	60
2.6.1 Structure and classes of biomolecules	60
2.7 Diagnostic kit of immunochromatographic (ICG) strip assay	63
2.7.1 History of rapid test	63
2.7.2 Theory on ICG strip assay	63
2.7.2.1 Sandwich format	65
2.7.2.2 Compete format	66
CHAPTER 3: METHODOLOGY	67
3.1 Introduction	67
3.2 Chemicals and Materials	68
3.2.1 Synthesis AuNPs	68
3.2.2 AuNPs conjugated to biomolecules	69
3.3.3 Development of ICG strip assay and testing on the strip	71
3.3 Protocols and parameters study of AuNPs conjugated biomolecules	72
3.3.1 Synthesis AuNPs	73
3.3.1.1 Seed stage	73
3.3.2.1 Growth stage	77
3.3.2 AuNPs conjugated biomolecules	79
3.3.3 Development of ICG strip assay	81
3.3.4 Performance and testing of ICG strip assay	83
3.4 Characterization methods	86

3.4.1 Transmission Electron Microscopy (TEM)	86
3.4.2 Ultraviolet-visible spectroscopy (UV-Vis spectroscopy)	87
3.4.3 Zetasizer Nanoparticle characterization	87
3.4.6 X-Ray diffraction (XRD)	88
3.4.7 High-resolution Transmission Electron Microscopy (HRTEM)	88
3.4.8 Immunochromatographic (ICG) strip assay	89
CHAPTER 4: RESULT AND DISCUSSION	91
4.1 Introduction	91
4.2 Synthesis AuNPs using one-step seeding-growth method	92
4.2.1 Formation of seeds AuNPs	92
4.2.1.1 Types of reducing agent	92
(a) Sodium borohydride	93
(b) Trisodium citrate	94
4.2.2 Growth formation of AuNPs	99
4.2.2.1 AuNPs from ~ 4 nm seeds (NaBH ₄ as reducing agent)	100
4.2.2.2 AuNPs grown from seeds (trisodium citrate as reducing agent)	102
(a) Effect of AuNPs seeds volume	102
(b) Effect concentration of hydroxylamine hydrochloride (NH ₂ OH.HCl)	106
(c) Effect volume of gold chloride	113
4.2.3 HRTEM image for AuNPs	117
4.2.4 Proposed mechanism in formation of AuNPs via the one-step seeding-growth method	118
4.3 AuNPs conjugated biomolecules	121

4.3.1 10 nm AuNPs conjugated biomolecules	121
4.3.2 40 nm AuNPs conjugated biomolecules	124
4.3.3 The effect of size and synthesis method of AuNPs conjugated mouse anti-human IgG ₄ (M α HIgG ₄) in detecting <i>Brugian filariasis</i> disease	127
4.3.2.1 Optimization concentration of antibody for conjugation of 20, 30 and 40 nm AuNPs	130
4.3.2.2 UV-Vis absorption of 20, 30 and 40 nm AuNPs before and after conjugation	132
4.3.3.3: Sensitivity and specificity performance of ICG strip assay	136
4.4 Proposed mechanism for AuNPs-biomolecules as a detector on ICG strip assay	142
CHAPTER 5: CONCLUSIONS AND SUGGESTIONS FOR FUTURE WORK	146
5.1 Conclusions	146
5.2 Suggestions for future work	148
REFERENCES	150
APPENDIX	174

LIST OF TABLES

	Page	
Table 2.1:	The relationship between the diameter (d) of the gold particle, the total number of the atoms and the percentage of surface atoms	14
Table 2.2:	Summary of the cellular toxicity of AuNPs with respect to particle size, shape and surface group	25
Table 2.3:	Sizes of AuNPs associated with addition of trisodium citrate	39
Table 2.4:	Comparison of average sizes of AuNPs synthesized using various reducing agents (in nanometer)	45
Table 2.5:	General mechanisms of formation colloidal AuNPs with varying type of reducing agent	47
Table 2.6:	Applications of ICG strip assay with emerging markets available	55
Table 2.7:	Summary of antibody family with respective properties	62
Table 3.1:	Starting chemicals and materials used to synthesis AuNPs	69
Table 3.2:	Starting materials used for conjugate AuNPs to biomolecules	70
Table 3.3:	Materials and chemicals and use to line antigen on the ICG strip assay	71
Table 3.4:	Varying amount trisodium citrate at the seed stage	74
Table 3.5:	Summary of the effect of parameter study at growth stage	78
Table 3.6:	Isoelectric point of biomolecules with specific pH of AuNPs	80
Table 3.7:	Antigen lined as control line towards respective biomolecules	83
Table 4.1:	Physical properties of AuNPs obtained from the seeding-growth method at the growth stage with varying volumes of gold seeds	104
Table 4.2:	Summary of particle size measurement of AuNPs with varying hydroxylamine hydrochloride concentration	110
Table 4.3:	AuNPs size and PDI values of samples obtained from the seeding-growth method at the seed and growth stages using 0.1M NH ₂ OH	113

Table 4.4:	Physical properties of AuNPs obtained from the seeding-growth method at the growth stage with varying concentration of gold chloride	115
Table 4.5:	UV-Vis absorption spectra of AuNPs with their respective concentration when volumes of gold chloride were tuned	116
Table 4.6:	Summary of UV-Vis absorption spectra measurements (from Figure 4.24) of 40 nm AuNPs before and after conjugated with their respective antigen and measured PDI value	125
Table 4.7:	Physical properties of AuNPs synthesized using the citrate reduction method and the seeding-growth method	129
Table 4.8:	UV-Vis absorption spectra of AuNPs before and after conjugation to IgG ₄ . AuNPs were synthesized using the citrate reduction method and seeding-growth method	135

LIST OF FIGURES

	Page
Figure 1.1:	Applications of AuNPs as a biosensor 2
Figure 1.2:	Schematic diagram of working principle and structure of ICG test strip for positive and negative result 3
Figure 2.1:	The size comparison of small particles 8
Figure 2.2:	Schematic illustration of nanostructure shapes 10
Figure 2.3:	Properties of AuNPs and its advantages in wide-range applications 11
Figure 2.4:	Various kinds of nanomaterials with (A) 0D spheres and clusters, (B) 1D nanofibers, wires, and rods, (C) 2D films, plates, and networks and (D) 3D nanomaterials 12
Figure 2.5:	Figure 2.5: Basic structure of face centered cubic unit cell 13
Figure 2.6:	(a) HRTEM images of single crystalline AuNPs with small-angle electron diffraction (SAED) pattern, (b) XRD analysis and (c) Tapping-mode AFM images of resolved [100] superlattices surface of AuNPs synthesized by the inverse micelle method 15
Figure 2.7:	TEM images of AuNPs reshaped at different temperatures 17
Figure 2.8:	Schematic of plasmon oscillation for a sphere, showing the displacement of the conduction electron charge cloud relative to the nuclei 18
Figure 2.9:	SPR of 22 nm, 48 nm and 99 nm spherical AuNPs 19
Figure 2.10:	AuNPs interaction and assembly with (A – B): Linear assembly driven by van der Waals forces and electrostatic interactions while (C – D) demonstrated the specific interaction between chemical moieties 21
Figure 2.11:	(a) General schematic representation of the stabilization forces in colloidal AuNPs (b) after citrate reduction 22
Figure 2.12:	Cell survival data upon exposure to AuNPs for 3 days; cell viability measured by MTT assay: (A) survival of cells exposed to 18 nm AuNPs (citrate-capped); (B) survival of cells exposed to 18 nm AuNPs (CTAB capped); (C) TEM images show the cells with AuNPs with inset the high 24

	magnification image of a small region in the cell cytoplasm containing AuNPs	
Figure 2.13:	Summary of silver nanostructures with six typical morphologies and their corresponding gold hollow nanostructures inset: the mechanism formation of gold nanohollow from silver template	27
Figure 2.14:	(a) The dependence of peak shift relative to the peak position obtained with water as the dispersion solvent on the refractive index (η) of surrounding medium. (b) UV-Vis extinction spectra of gold solid colloids and gold nanoshells	28
Figure 2.15:	TEM images of CTAB coated Au particles in the presence of NaOH with irradiation time (a) 2 h, (b) 7 h, (c) 12 h and (d) 17 h	29
Figure 2.16:	TEM images of the AuNPs synthesized by photochemical method using X-ray irradiation: (a) without TX-100, inset is SAED pattern revealing the cubic structure of gold metal and (b) with TX-100	30
Figure 2.17:	TEM images of AuNPs produced via UV-irradiation method with (a) seeds Au synthesized using UV-irradiation and (b-d) Au after growth using ascorbic acid as reductant	31
Figure 2.18:	The TEM images of AuNPs prepared by sonochemical method (a) in the mixture solution of ethanol/water (180 min) and (b) in ethylene glycol (60 min). (c) UV-Vis absorption spectra for (b) samples	32
Figure 2.19:	(a) Synthesis mechanism of AuNPs by <i>Stenotrophomonas maltophilia</i> and (b) TEM image of produced AuNPs with inset the red suspension colloidal AuNPs	33
Figure 2.20:	TEM images of Au nanoparticles produced at (a) pH 1, (b) pH 2, (c) pH 3, (d) pH 4 and (e) pH 5	34
Figure 2.21:	TEM images of different shaped Au nanostructures synthesized after 90 seconds of MW exposure with (A) image of spherical AuNPs; (B) low magnified images of mixed (mixture of different shapes) shaped AuNPs; C and D show the images of Au nanorods at different magnification. The inset of A show the corresponding electron diffraction of the particles and a higher magnified image	35
Figure 2.22:	(a-b) TEM images of 10 nm AuNPs produced via solvent evaporation approach. TEM images of AuNPs after undergo solubility process on water with (c) sponge-like structures and (d) wires of AuNPs formed via electrostatic interactions	38

between oppositely charged nanoparticles

- Figure 2.23: TEM results for two of the AuNPs; (a) 24 nm and (b – c) 41 nm with red suspension liquid. Size bars are 100 nm for both images. (d) Blue-grey of 147 nm AuNPs when 0.30 mL of 1% trisodium citrate used 39
- Figure 2.24: Formation mechanism of AuNPs with various particle sizes and shapes by chemical reduction route with specific seeding-growth method 40
- Figure 2.25: Representative TEM images. (A) Au@citrate at seed stage ($d=10.8 \pm 0.8$ nm). At growth stage: (B) first generation ($d = 18.0 \pm 1.8$ nm) and (C) second generation nanoparticles prepared in (1) 0.10, (2) 0.30, (3) 0.50, (4) 0.70, (5) 0.90 and (6) 1.10 mM citrate concentrations, respectively 42
- Figure 2.26: Mechanism of AuNPs produced by seeding-growth method proposed by Brown and Natan 43
- Figure 2.27: (a – f) TEM images of AuNPs reduced from ascorbic acid via seeding-growth method. (g) Experimental set-up of the experiment 44
- Figure 2.28: TEM images of as-made different-sized gold nanoparticles produced by temperature (A) 2.1 ± 0.3 nm; (B) 3.5 ± 0.3 nm; (C) 5.3 ± 0.4 nm; (D) 6.2 ± 0.3 nm; (E) 7.1 ± 0.5 nm; (F) 8.3 ± 0.5 nm. All scale bars are 20 nm 49
- Figure 2.29: Schematic illustration of the formation and stability of the AuNPs and their morphology change in the pH of the solution 50
- Figure 2.30: Various states and configurations of particles in dry state and when dispersed 52
- Figure 2.31: Figure 2.31: TEM images of AuNPs for various concentration of 100 mL HAuCl₄ solution used 53
- Figure 2.32: Planar X-ray images of AuNPs (a–d) and iodine contrast agent (e–h) in live mice. Before injection (a, e); 2 min after injection (b, f); 10 min after injection (c, g) and 60 min after injection (d, h) with inset (d', h') are the closet images. The AuNPs show low liver and spleen uptake and clearance via kidneys and bladder (b–d) 57
- Figure 2.33: (a – b) Principle of selective laser killing of *S. Aureus* targeted with AuNPs. TEM images of (c) bacteria attached with 40 nm AuNPs before PT, (d) bacteria alone after PT, (e) bacteria attached with 40 nm AuNPs after 30 nanosecond PT and (f) bacteria attached with 40 nm AuNPs after 120 58

nanosecond PT

Figure 2.34:	(a) Schematic representation of the preparation of an immunosensing layer. (b) Schematic view of electrochemical detection of mouse IgG conjugated 10 nm AuNPs	60
Figure 2.35:	The ICG strip structure: (A) Schematic representation of the ICG strip assay. (B) Lateral (top) and over (bottom) views of an ICG strip. The outmost layers of the ends of the strip are plastic cover films	64
Figure 2.36:	Principles of the ICG test strip assay in sandwich format	66
Figure 2.37:	Principal of ICG test strip assay in competitive format	66
Figure 3.1:	Flowchart of overall experiment with parameters studied	72
Figure 3.2:	Colour changes during synthesis of seeds AuNPs: a) heating and stirring gold chloride solution, b) upon addition 1% (w/v) trisodium citrate, c) 15 second after addition, d) 30 second after addition, e) 50 second after addition, f) 1 minute after addition, g) 2 minutes after addition and h) reduction of AuNPs completed	75
Figure 3.3:	Flow chart of experimental works to synthesize seeds AuNPs using sodium borohydride and trisodium citrate as a reducing agent	76
Figure 3.4:	Flow chart of experimental procedure to synthesis AuNPs at growth stage	79
Figure 3.5:	Schematic diagram of working principle and structure of ICG test strip. A: experimental set-up, B: top view and C: cross-section of the strip	82
Figure 3.6:	General protocol for conjugation process and testing on ICG strip assay	85
Figure 3.7:	Schematic diagram of analyzing ICG strip assay performance after tested with serum	89
Figure 3.8:	Isoflow dispenser machine used for lining ICG strip assay	90
Figure 4.1:	(a) Particle size distribution by volume with inset the AuNPs seeds after reduction with NaBH ₄ , (b) UV-Vis spectrum of AuNPs seeds	94
Figure 4.2:	TEM images of AuNPs seeds with varying volumes 1% w/v of trisodium citrate: (a) 1.0, (b) 1.4, (c) 1.6, (d) 2.0 and (e) 5.0 ml	95

Figure 4.3:	Histograms of particle size distribution of AuNPs from TEM images at seed stage. (a) – (e) are corresponded to Figure 4.2 (a) – (e) respectively with black line represent major axis (long direction) and grey line represent minor axis (short direction)	96
Figure 4.4:	Polydispersity index (PDI) of AuNPs seeds with varying volume of 1% trisodium citrate	97
Figure 4.5:	XRD pattern of AuNPs seeds synthesized using trisodium citrate as a reducing agent	98
Figure 4.6:	Schematic mechanism of AuNPs seeds formation from gold ions (Au^{3+}) to gold atom (Au^0) using trisodium citrate as a reducing agent	99
Figure 4.7:	TEM images with respective histograms of particle size distribution of AuNPs after the growth process with (a) 7 ml seeds (b) 4 ml seeds and (c) 1 ml seeds	100
Figure 4.8:	(a) UV-Vis absorption spectra of seeds and growth AuNPs grown from 1, 4 and 7 ml of seeds. (b) PDI value of AuNPs grown from seeds AuNPs	101
Figure 4.9:	Morphology of AuNPs after varied volume of seeds at growth stage with (a) 0.5 ml, (b) 1.5 ml (c) 2.5 ml (d) 5 ml (e) 10 ml and (f) the seeds of AuNPs. (g) Measurement dimension of major (x) – axis and minor (y) – axis	103
Figure 4.10:	UV-Vis spectra of AuNPs produced by varying volume of seed solution at the growth stage	105
Figure 4.11:	XRD pattern of AuNPs synthesized by tuning volumes of seeds solution	106
Figure 4.12:	AuNPs produced when the concentrations of hydroxylamine were varied from 0.1 M to 3 M	107
Figure 4.13:	TEM images of AuNPs with varying hydroxylamine hydrochloride concentrations: (a) 0.1 M, (b) 0.2 M, (c) 0.7 M, (d) 2 M and (e) 3.0 M (inset is a larger magnification of AuNPs). (f) 20 nm AuNPs seeds used	109
Figure 4.14:	Crystallinity of AuNPs when concentrations of NH_2OH were varied using XRD analysis	111
Figure 4.15:	AuNPs grown from 15 nm seeds with final diameter of AuNPs is (a) 20, (b) 30, (c) 40, (d) 50, and (e) 60 nm. (f) Images of AuNPs seeds	112

Figure 4.16:	TEM images of AuNPs with varying volume of gold chloride at the growth stage: (a) 0.25 ml, (b) 0.5 ml (c) 1.0 ml (d) 2.0 ml and (e) 3.0 ml. (f) Images of AuNPs seeds used for the growth stage	114
Figure 4.17:	UV-Vis spectra of AuNPs resulting from with varying volume of gold chloride at the growth stage	116
Figure 4.18:	XRD spectra of AuNPs with varying concentration of gold chloride from 0.25 mL to 3.0 mL	117
Figure 4.19:	HRTEM images of 30 nm AuNPs (a) general image, (b) lattice fringes for atomic arrangement observed at higher magnification	118
Figure 4.20:	Schematic illustration of AuNPs formation synthesized using the seeding growth method. AuNPs were grown using seeds reduced by (a) sodium borohydride and (b) trisodium citrate. (c – d) Growth stage of AuNPs	120
Figure 4.21:	Optimization amount of streptavidin to 1 ml 10 nm. 10 μ g/ml of streptavidin to 1 ml of 10 nm AuNPs was obtained as the optimum concentration for conjugation	122
Figure 4.22:	(a) UV-Vis absorption spectra of 10 nm AuNPs before and after conjugation with streptavidin and goat anti-human IgA. (b) 10 nm AuNPs conjugated streptavidin and (c) 10 nm AuNPs conjugated goat anti-human IgA labelled on ICG strip assay detection zone	123
Figure 4.23:	Optimization of BSA concentration as stabilizer during conjugation of 10 nm AuNPs (OD 4) to goat anti-human IgA	124
Figure 4.24:	UV-Vis absorption spectra of 40 nm AuNPs before and after conjugation with biomolecules	125
Figure 4.25:	Size distribution of 40 nm AuNPs after conjugation by intensity measured by Zeta-sizer measurement with respective hydrodynamic size (Z_{ave})	126
Figure 4.26:	40 nm AuNPs conjugated biomolecules as detector on ICG strip	126
Figure 4.27:	Final solution of colloidal 20, 30 and 40 nm AuNPs after synthesized using (a) citrate reduction method and (b) seeding-growth method	128
Figure 4.28:	Concentration gradient of AuNPs / M α HIgG ₄ mixtures after incubation. The three tubes on the left contain insufficient	131

amount of M α HIgG₄ to stabilize AuNPs when 10% NaCl was added. The optimum concentration of M α HIgG₄ to stabilize AuNPs is the fourth tube while the fifth tube contains excess M α HIgG₄. The 20, 30 and 40 nm AuNPs produced using the citrate reduction method are labelled as (a), (b) and (c) respectively, while the 20, 30 and 40 nm AuNPs produced using the seeding-growth technique are labelled as (d), (e) and (f), respectively

- Figure 4.29: UV-Vis absorption spectra of AuNPs before (grey line) and after conjugated to M α HIgG₄ (black line) using synthesized method of AuNPs (a) citrate reduction method and (b) seeding-growth method 133
- Figure 4.30: AuNPs- M α HIgG₄ labelled ICG strips with varying test line (*BmR1* recombinant antigen) concentrations: (a) 0.75 mg/ml, (b) 1.0 mg/ml and (c) 1.5 mg/ml 136
- Figure 4.31: Size effect of AuNPs conjugated with M α HIgG₄ on colour intensity of the test line of developed ICG test strip as in inset 137
- Figure 4.32: Total time performance of immunchoromatographic (ICG) test strip tested with positive serum (from inset figure) 139
- Figure 4.33: Comparison of the sensitivities of 30 nm and 40 nm AuNPs– M α HIgG₄ on ICG strips in detecting antibody in increasing dilutions of a positive serum sample (30 and 40 nm AuNPs produced using the seeding-growth method) 140
- Figure 4.34: ICG strip of varying OD of 30 nm AuNPs– M α HIgG₄ tested with positive serum at 1: 128 dilutions 140
- Figure 4.35: ICG strip of 30 nm AuNPs–M α HIgG₄ at OD 4 tested with different types of serum samples (a) high positive (HPS) and low positive (LPS) serum samples from *Brugian filariasis* patients; (b) negative (control) serum samples comprising NI and N2 from patients with mixed roundworm infections i.e. *Trichuris trichiura* and *Ascaris lumbricoides*; N3 and N4: from patients with single roundworm infection i.e *Trichuris trichiura*; N5 from a patient infected with *Entamoeba histolytica* 141
- Figure 4.36: Schematic diagrams of working principle and structure of ICG test strip with conjugation process of AuNPs–biomolecules and inset illustrated the assay in sandwich format and results interpret for ICG strip 145

LIST OF ABBREVIATIONS

Abbreviations	Compound
Ab	Antibodies
AuNPs	Gold nanoparticles
AuNPs-M α HIgG ₄	Gold nanoparticles conjugated mouse anti-human IgG ₄
BmR1	<i>Brugia malayi</i> Reagent 1
ELISA	Enzyme-linked Immunosorbent Assay
FCC	Face-centered cubic
Fc-D	ferrocenyltethered dendrimer
HAuCl ₄	Chloroauric acid / gold chloride / gold salt
hBMSCs	Human bone marrow mesenchymal stem cells
hCG	Human chorionic gonadotropin
HCP	Hexagonal close-packed
HCV	<i>Hepatitis C</i> virus
HIV	<i>Human Immunodeficiency</i> virus
HPS	High positive serum
HRTEM	High-resolution transmission electron microscopy
HuH-7	Human hepatoma carcinoma cells
ICG	Immunocharomatographic
IEP	Isoelectric point
ITO	indium tin oxide
JCPDS	Joint Committee on Powder Diffraction Standards
LFI	Lateral flow immunoassay
LPS	low positive serum

M α HIgG ₄	Mouse anti-human IgG ₄
MTT	Microculture Tetrazolium
MWI	Microwave irradiation method
M _w	Molecular weight
NC	Nitrocellulose
OD	Optical density
PDI	Polydispersity index
PT	Photothermal therapy
SAED	Selected Area Electron Diffraction
SHE	Standard hydrogen electrode
SMAD	Solvated metal atom dispersion
SPR	Surface plasmon resonance
TEM	Transmission electron microscopy
UV-Vis	Ultraviolet – Visible
X-ray CT	X-ray Computed Tomography
XRD	X-Ray Diffraction
Z _{ave}	Hydrodynamic size

LIST OF SYMBOLS

nm	Nanometer
μ l	Microliter
ml	Milliliter
mm	millimeter
λ	Wavelength
$^{\circ}$ C	Degree celcius
L	Length
d	Diameter
M	Molarity
V	Volume
η	Refractive index
h	hour
%	Percent
rpm	Revolutions per minute
g	gram
g	Gravity force
G	Degree of ellipticity
σ	Standard deviation
v/v	Volume per volume
w/v	Weight per volume
θ°	Theta
Ω	Ohm / resistance

List of Publications

Siti Rabizah Makhsin, Khairunisak Abdul Razak, Rahmah Noordin, Nor Dyana Zakaria and Tan Soo Chun, The effects of size and synthesis methods of gold nanoparticle-conjugated M α HIgG₄ for use in an immunochromatographic strip test to detect brugian filariasis, *Nanotechnology* (2012), 23 pp. 495719 (IF=3.979)

Ooi, P. C., Aw, K. C., Razak, K. A., Makhsin, S. R. & Gao, W. Effects of Metal Electrodes and Dielectric Thickness on Nonvolatile Memory with embedded Gold Nanoparticles in Polymethylsilsequioxane, *Microelectronic Engineering* (2012), Vol. 98, p. 74-79 (IF=1.495)

Siti Rabizah Makhsin, Khairunisak Abdul Razak, Azlan Abdul Aziz, Rahmah Noordin, Study on Controlled Size, Shape and Dispersity of Gold Nanoparticles (AuNPs) Synthesized via Seeded-growth Technique for Immunoassay Labeling, *Advanced Materials Research*, Vol. 364, 2012, 504-509

Khairunisak Abdul Razak, Siti Rabizah Makhsin, Teoh Poay Ling, Nordyana Zakaria, Rahmah Noordin, Seeding growth of gold nanoparticles and their properties in diagnostic application, 21st Scientific conference of the Microscopy Society Malaysia, 22-24 November 2012, Kota Bharu, Kelantan, Malaysia, p. 37

Siti Rabizah Makhsin, Khairunisak Abdul Razak, Azlan Abdul Aziz, Rahmah Noordin, Green Synthesis of 10 nm Gold Nanoparticles via Seeded-growth Method and its Conjugation Properties on Lateral Flow Immunoassay, 8th International Materials Technology Conference and Exhibition (IMTCE 2012), 7 – 12 July 2012, Sunway Resort Hotel & Spa, Selangor, Malaysia, p. 57

Siti Rabizah Makhsin, Khairunisak Abdul Razak, Azlan Abdul Aziz, Rahmah Noordin, The Effect of Gold Nanoparticles Size Conjugated Mouse Antihuman IgG₄ in Immunochromatographic Strip Assay for *Brugian Filariasis* Detection, 4th Regional Conference On Molecular Medicine (RCMM) 2011, 9 - 11 October 2011, G - Hotel, Penang, Malaysia, p. 83

Siti Rabizah Makhsin, Khairunisak Abdul Razak, Azlan Abdul Aziz, Rahmah Noordin, Study on Controlled Size, Shape and Dispersity of Gold Nanoparticles (AuNPs) Synthesized via Seeded-Growth Technique for Immunoassay Labeling, The International Conference for Nanomaterials Synthesis and Characterization 2011 (INSC 2011), 4 – 5 July 2011, Mines Wellness Hotel, Selangor, p. 45

SIFAT NANOPARTIKEL EMAS DAN KONJUGATNYA DENGAN BIOMOLEKUL UNTUK KEGUNAAN DIAGNOSTIK

ABSTRAK

Dalam kajian ini, nanopartikel emas (AuNPs) koloid telah disintesis menggunakan kaedah pembenihan-pertumbuhan. Kaedah ini bermanfaat untuk menghasilkan AuNPs berbentuk sfera dalam pelbagai saiz daripada 6 nm – 150 nm dengan indeks polidispersiti (PDI) kurang daripada 0.2 apabila kuantiti benih diubah. AuNPs disintesis menggunakan kaedah ini juga sudah tersedia untuk konjugasi dan memerlukan kepekatan antibodi yang rendah (~50% kurang) untuk digunakan pada imunokromatografi (ICG) jalur ujian berbanding kaedah konvensional, sekali gus mengurangkan kos penghasilan ICG jalur. Natrium borohidrida dan trisodium sitrat digunakan sebagai agen penurunan untuk mendapatkan benih AuNPs bersaiz 4 nm – 40 nm. Kepekatan optimum hidrosilamin (NH_2OH) sebagai agen penurunan pada peringkat pertumbuhan adalah pada 0.1 – 0.2 M. Larutan AuNPs berkepekatan tinggi dalam pelbagai saiz (35 nm – 90 nm) dengan tahap eliptisiti (G) ≤ 1.09 diperoleh apabila isipadu emas klorida diubah daripada 0.25 ml ke 3 ml. Saiz-saiz AuNPs yang terpilih (10 nm and 40 nm) berjaya dikonjugasi dengan biomolekul dan terbukti sebagai pengesan yang baik pada ICG jalur ujian. Sifat AuNPs (saiz: 20, 30 dan 40 nm) disintesis melalui kaedah pengurangan sitrat dan pembenihan-pertumbuhan dikonjugasi dengan *mouse anti-human IgG₄* ($\text{M}\alpha\text{HIgG}_4$) untuk mengesan penyakit *Brugian filariasis* menggunakan ICG jalur ujian telah dibandingkan. 30 nm AuNPs- $\text{M}\alpha\text{HIgG}_4$ dengan ketumpatan optik (OD) 4 daripada kaedah pembenihan-pertumbuhan menunjukkan prestasi yang terbaik untuk digunakan dalam pelabelan ICG jalur ujian apabila menunjukkan sensitiviti terbaik dan spesifisiti tertinggi apabila diuji dengan sampel serum dari *Brugian filariasis* pesakit dan kawalan.

PROPERTIES OF GOLD NANOPARTICLES AND ITS CONJUGATION WITH BIOMOLECULES FOR DIAGNOSTIC APPLICATION

ABSTRACT

In this study, colloidal gold nanoparticles (AuNPs) were synthesized using the seeding-growth method. This approach was beneficial to produce spherical shape AuNPs with the size range from 6 nm to 150 nm with polydispersity index (PDI) below 0.2 by varying the volume of seed solution. AuNPs synthesized using this method also are readily available for conjugation and require lower antibody concentration (~50% less) when applied to the immunochromatographic (ICG) strip assay compared to conventional method, thus significantly reduce the ICG strip production cost. Sodium borohydride and trisodium citrate were used as reducing agent to obtain 4 nm – 40 nm AuNPs seeds. The optimum concentration of hydroxylamine as a reducing agent at the growth stage was 0.1 to 0.2 M. High concentration of AuNPs solution with tunable size (35 nm – 90 nm) with the degree of ellipticity ($G \leq 1.09$) was obtained when volume of gold chloride were tuned from 0.25 ml to 3 ml. Selected sizes of AuNPs (10 nm and 40 nm) were then successfully conjugated to biomolecules and proved to work well as detector on ICG strip assay. The properties of AuNPs (sizes: 20, 30 and 40 nm) synthesized using the citrate reduction and seeding-growth methods and their conjugation to mouse anti-human IgG₄ (M α HIgG₄) to detect *Brugian filariasis* disease using ICG strip assay were compared. The 30 nm AuNPs-M α HIgG₄ with optical density (OD) 4 from the seeding-growth method showed the best performance for use in labelling ICG strips assay since it displayed the best sensitivity and the highest specificity when tested with serum samples from *Brugian filariasis* patients and controls.

CHAPTER 1

INTRODUCTION

1.1 Introduction

Gold nanoparticles (AuNPs) with sizes ranging from 10 to 100 nm are known to have a large light absorption and scattering in the surface plasmon resonance wavelength regions. AuNPs are also known as colloidal gold are the most stable metal nanoparticles. AuNPs are of interest due to their unique features including properties of individual particles, assembly of multiple types, size-related electronic, magnetic and optical properties and their great potential applications in various fields (Daniel and Astruc, 2004b). The magnitude of light scattering by AuNPs can be in order of magnitude higher than light emission from strong fluorescence dyes (Rasch *et al.*, 2009, Liu *et al.*, 2008). The Au surface provides protection against oxidation and helps to maintain long-term stability. In addition, Au in nano-size offers high surface area and unique physical-chemical properties that can be easily tuned. AuNPs are excellent candidates for surface functionalization as they are easily synthesized, biocompatible, easily attached to molecules and able to mobilize in biological systems (Sokolov *et al.*, 2003, Kim *et al.*, 2007). These unique properties have enabled many important and promising applications of AuNPs especially in biomedical field such as biosensor, diagnostic imaging, molecular and cancer cell biomarker imaging and photothermal (Day *et al.*, 2010, Kim *et al.*, 2007, Nguyen *et al.*, 2011). Among these applications, biosensor consisting of AuNPs as one of the important component during its fabrication is of interest. Biosensor modified with AuNPs has enhanced its performance as illustrated in Figure 1.1. The presence of

AuNPs in the biological test makes the activity of analytes become quicker, more sensitive and flexible compared to the traditional procedures (Vidotti M, 2011).

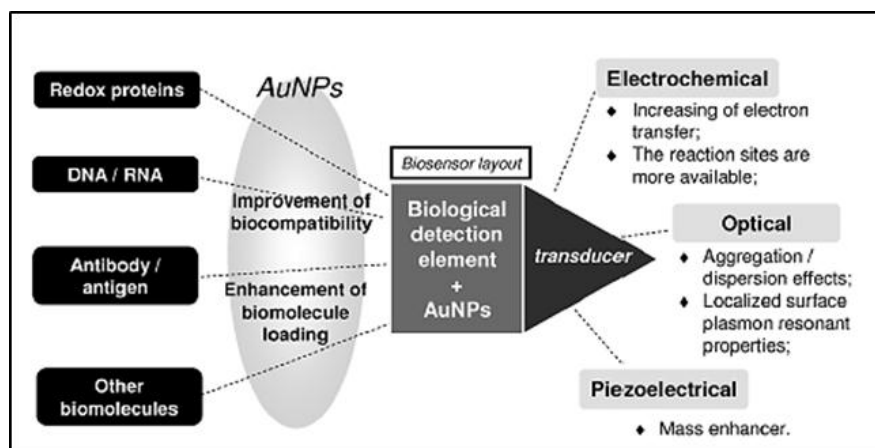


Figure 1.1: Applications of AuNPs as a biosensor (Vidotti M, 2011)

In recent years, the development of immunoassay in a “lateral flow test format” based on immunochromatography principle for the detection of specific diseases has gained interest as a rapid ‘point-of-care’ test which can be transported at room-temperature (Kaur *et al.*, 2007). The result can be visually observed and easily interpreted, thus allows the diagnostic test to be performed in the field which have advantages of high sensitivity, high specificity and user-friendly analysis (Zhang *et al.*, 2006). Hence, the immunochromatographic (ICG) tests using AuNPs-conjugated proteins are attractive materials for development of biosensors such as lateral flow diagnostic test (Naoki *et al.*, 2006, Xiulan *et al.*, 2005). The basic working principle of ICG strip assay used in this study is based on the sandwich assay as illustrated in Figure 1.2. The analytical signals are observed after a specific interaction of the ligand and the analytes such as an antigen-antibody complex. This specific interaction takes place in the membrane by capillary effect of the medium. In one format of an antibody detection test, the antigen is immobilized on the membrane

while a secondary antibody is conjugated with the AuNPs (Tanaka *et al.*, 2006). The antibody in the sample binds with the immobilised antigen (test line) and this antigen-antibody complex then binds to the detector secondary antibody conjugated with AuNPs. The red color visualized is caused by the accumulation of the AuNPs at that location of test and control lines on the membrane (Kaur *et al.*, 2007, Naoki *et al.*, 2006).

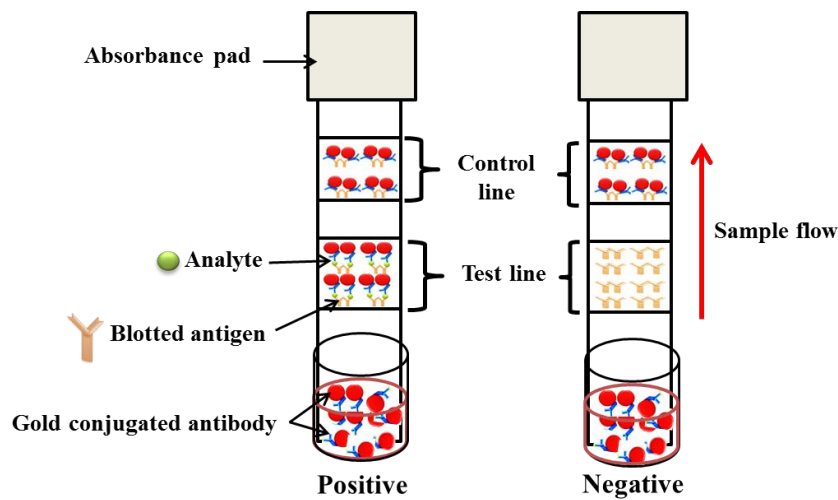


Figure 1.2: Schematic diagram of working principle and structure of ICG test strip for positive and negative result

1.2 Research motivation

AuNPs in the colloidal form becomes attractive nowadays due to the superior properties of this noble metal especially in biomedical application. The excellent properties of colloidal AuNPs only can be achieved by optimizing the synthesis method of AuNPs. Although there are many methods to produce spherical AuNPs, most previous works cannot produce AuNPs with the following features: impeccable spherical shape, monodisperse, nontoxic and easy to exchange stabilizer and reductant, excellent size distribution, does not require post synthetic cleanup and simple set up. In this research, a novel approach to overcome the weaknesses of the

seeding-growth method by using hydroxylamine (NH_2OH) as a reducing agent that forms monodisperse structure of AuNPs with completely spherical shape, simple and quick process and without post synthetic cleanup. The major finding in this result also improves the research outcome from Brown *et al.* (2000) whereby their works shows that the seeding-growth method with NH_2OH led to the formation of a small percentage of cylindrical with high aspect ratio of rods. Also, the seeding- growth method has advantages of high repeatability and low cost experimental set-up compared to other methods.

There are a lot of reports on the use of AuNPs in the ICG strip test. Most previous reports used a well-known method citrate reduction method to synthesis AuNPs with varying sizes using trisodium citrate as the reducing agent (Xiulan *et al.*, 2005, Tian *et al.*, 2009, Khreich, 2008, Tang, 2011, Zhang *et al.*, 2006). This method is easy but the major drawback is that the spherical gold tends to have an elliptical shape when the size exceeds 30 nm and produces poly-dispersed particles (Brown *et al.*, 2000). In order to overcome these drawbacks, the seeding-growth method to synthesis various sizes of AuNPs was introduced by Brown and Natan (Brown and Natan, 1998). The dimension and shape of the nanoparticles can be controlled whereby the size can be predetermined by allowing smaller particles to grow into larger particles in the seeding-growth method. The particles produced are more mono-dispersed compared to the citrate reduction method. To the author's knowledge, there are very limited works on using of AuNPs synthesized using the seeding-growth method to label biomolecules. In addition, AuNPs produced using this method are readily available for conjugation with biomolecules through surface absorption and require fewer concentration of antibody for ICG strip assay

application compared to the citrate reduction method. Moreover, the seeding-growth method also provide a specific interaction on AuNPs surface to biomolecules site through ionic bond (NH_2^-) whereby this binding will improve the sensitivity of the conjugated AuNPs as detector on labelling ICG strip assay.

The novelty of this work lies on conjugation of AuNPs synthesized using seeding-growth method to antibody and its properties compared to the well-known citrate reduction method. The present case study is on a test for *Brugian filiarisis* which is a neglected tropical disease in developing countries. Thus the result of this study will be of practical importance in helping to reduce the price of diagnostic kits for these resource-poor areas, in addition to benefitting the lateral flow test industry in general. To date, most diagnostic kits use 40 nm AuNPs, but in this study we have proven that 30 nm AuNPs is the optimum size for detection in ICG strip assay. It is known that for ICG strip, 80% of the cost is that of the antibody. In this study we have shown that AuNPs produced using the seeding-growth technique requires less antibody (~50% lesser) than AuNPs produced using citrate reduction method, hence this will significantly reduce the production cost.

1.3 Objectives

The main objectives of this research involve:

1. To optimize synthesis parameters on formation of AuNPs using the seeding-growth techniques.
2. To study conjugation of AuNPs with various types of biomolecules.
3. To test selected conjugated products in an ICG test strip assay for diagnostic kit application.

4. To optimize conjugated gold nanoparticles to antibody as detection agent in ICG strip assay.

1.4 Scope of the work

In this work, AuNPs in a spherical shape were synthesized using the seeding-growth method and the citrate reduction method. The effects of several synthesis parameters were studied in order to understand the formation mechanism. The size and shapes of AuNPs were observed using a transmission electron microscopy (TEM). The atomic arrangement of single particle AuNPs was studied using high-resolution TEM (HRTEM). The optical properties of AuNPs were studied using UV-Vis spectroscopy. The phase presence in AuNPs was characterized using X-Ray Diffractometer. The dispersity and hydrodynamic size of AuNPs were studied by using Zeta-sizer measurement. Several sizes of AuNPs were then conjugated to biomolecules (goat anti-human IgM, goat anti-human IgA, goat anti-human IgG and streptavidin) and tested with ICG strip assay to study the binding properties and interaction behavior between AuNPs and biomolecules. The UV-Vis absorption spectrum was used to obtain the concentration and determine the stability of the AuNPs conjugated biomolecules. The effect of size (20, 30 and 40 nm) and synthesis method (citrate reduction and seeding-growth method) on AuNPs conjugation as a detector on ICG strip assay was studied in detail.

1.5 Dissertation structure

This dissertation is organized as follows: In chapter 1, the introduction, objectives, research motivation, and scope of the work are presented. In Chapter 2, the literature review related to the background of the project is described. The

experimental works are explained in details in Chapter 3. Results and discussion of this works are systematically explained in Chapter 4. Lastly, conclusion and suggestions for a future works are included in Chapter 5.

CHAPTER 2

LITERATURE REVIEW

2.1 Introduction of Nanobiotechnology

Nanotechnology is combination of science, engineering and technology conducted at the nanoscale, which is about 1 to 100 nanometers (nm). The scale of nano is about 10^{-9} and contains atoms in range of 10^2 to 10^7 atoms as illustrated in Figure 2.1 (Murray *et al.*, 2000). It is expected that nanotechnology will be developed at several levels covering world of advanced materials, devices and systems (Salata, 2004).

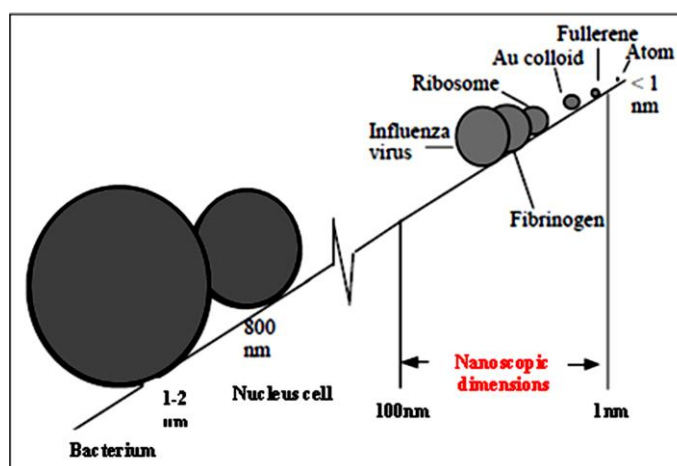


Figure 2.1: The size comparison of small particles (Richards, 2001)

The term nanobiotechnology or frequently interchangeable with bionanotechnology is the branch of nanotechnology that combines with biological and biochemical to meet certain applications. If the two are distinguished, nanobiotechnology usually refers to the use of nanotechnology to further the goals of biotechnology, while bionanotechnology refers to any overlap between biology and

nanotechnology including the use of biomolecules such as nucleic acid and DNA as part of or as an inspiration for nanotechnological devices. Nanobiotechnology also can be defined as a detection of proteins and inhibitors, emphasizing their active binding sites by using nanoparticles (Kostoff *et al.*, 2006). Nowadays, nanobiotechnology field is rapidly growing in most advance area of scientific and technology to create a huge potential in fabrication nano-devices especially in biosystems. Nanobiotechnology often involves studies on existing elements of nature such as biomolecules in order to fabricate new devices (Brooks *et al.*, 1983).

Major applications of nanosystem can be found in biomedical fields. Nanosystems are often accumulated at higher concentration than normal drugs, thereby enhancing bioavailability at the targeted site (Chen, 2008). In addition, the capability of nanoparticles to enhance drug targeting to the diseased tissues can lead to reduction of systemic toxicity. Besides, with the help of nanomaterials, the solubility of drug will be enriched so that the regulated drug release with improved retention at the target sites will be obtained. These unique properties of nanosystem can be exploited to deliver drugs to harder-to-target sites such as brain area and there is a great potential to solve the blood-brain barrier by introducing nanomaterials into the system (Jain *et al.*, 2008, Caban *et al.*, 2012). The most interesting features about nanomaterials to be explored more a decade ago are due to their shape, size-dependent physical and chemical properties (Murray *et al.*, 2000). The geometric features such as size and shape of nanomaterial extremely affect its properties and behaviour compared to when it is in micron size (Carbone and Cozzoli, 2010). Each size and shape of nanomaterials affect the properties of the materials including physical (Daniel and Astruc, 2003), optical, photothermal, biological (Eustis and El-

Sayed, 2006), mechanical, electrical (Maysinger, 2007), and chemical activity (Bakshi *et al.*, 2008). Among these, the most important factor to play a role in determining the properties of nanomaterials is shape effect (Daniel and Astruc, 2004a). The common shapes of nanoparticles synthesized nowadays are summarized in Figure 2.2.

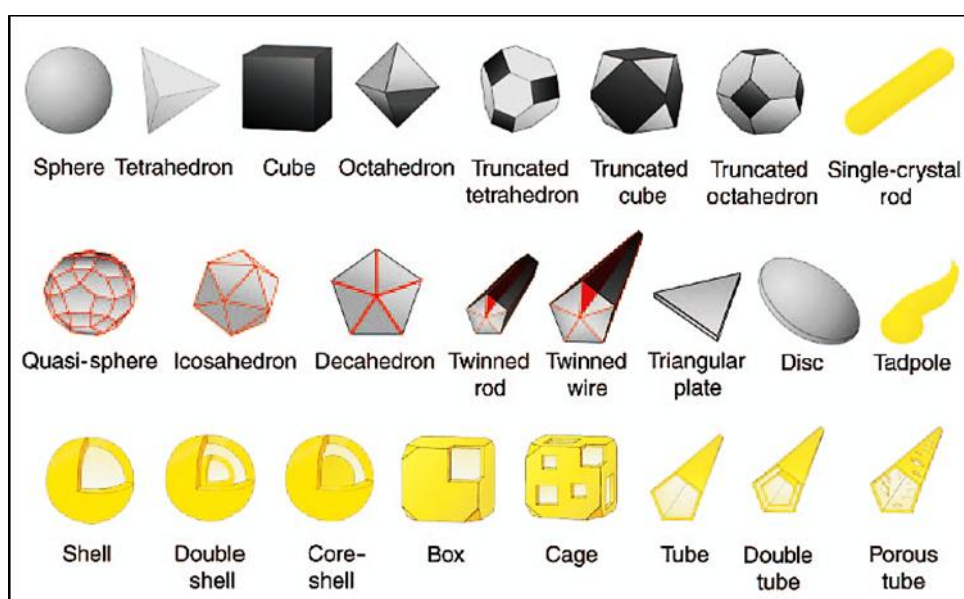


Figure 2.2: Schematic illustration of nanostructure shapes (Younan *et al.*, 2005)

In the world of nanobiotechnology, nanomaterials must meet requirements for biomedical applications such as non-toxic, biocompatible, stable in biological environment and reactivity in biological environment (Jain *et al.*, 2008). The utilization of nontoxic chemicals, environmentally benign solvents and renewable materials are emerging issues that merit important consideration in the development of synthetic strategies in producing noble nanomaterials (Reijnders, 2008, Şengül *et al.*, 2008). Some nanomaterials such as gold nanoparticles (AuNPs) have been identified to meet all the demands as a prominent nanomaterial for nanobiotechnology applications. This inorganic material, AuNPs is easily attached

with biomolecules especially with protein via surface absorption. Carbone and Cozzoli (2010) suggested that most inorganic nanomaterials are preferentially bound with biomolecules via surface absorption.

2.2 Gold Nanoparticles (AuNPs)

Metal nanoparticles, particularly AuNPs are being considered in wide ranges of applications such as photonics, information storage, electronic and optical detection systems, therapeutics, diagnostics, photovoltaics, and catalysis (Alexandridis, 2010). AuNPs are the most stable metal nanoparticles with fascinating features such as size-related electronic, optical properties and capability as catalysis for biological and chemical system. AuNPs also have capability to be used as protein detection and behave as inhibitors by emphasizing their active binding sites (Kostoff *et al.*, 2006). Moreover, AuNPs have an ability to provide stable immobilization process of biomolecules by retaining their bioactivities (Nguyen *et al.*, 2011). In addition, AuNPs also exhibit strong surface plasmonic resonance and commonly used to coat other nanomaterials such as iron oxide, silica and silver nanoparticles as illustrated in Figure 2.3 (Jans and Huo, 2012).

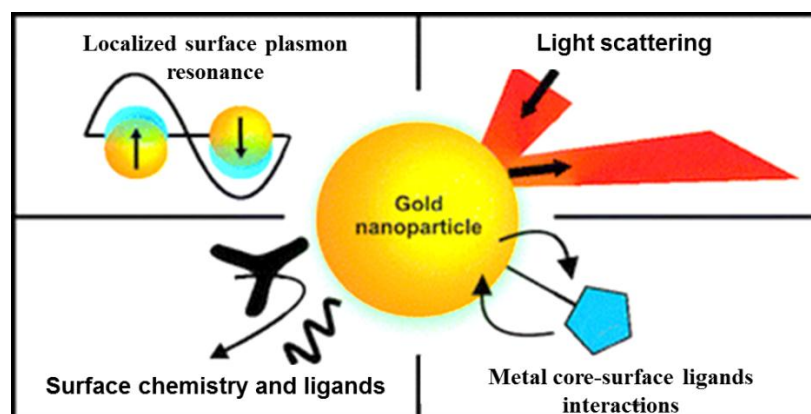


Figure 2.3: Properties of AuNPs and its advantages in wide-range applications (Jans and Huo, 2012)

2.2.1 Structures of AuNPs

Generally, the changes in properties of AuNPs are due to the structures and physical shape of an object which are influenced by restricted motion of electrons, holes, excitons, phonons and plasmons (Sajanlal *et al.*, 2011). The most important change of AuNPs that is clearly observed is color. The color changes are due to the confinement of electrons and consequent changes in electronic energy levels. The structure of AuNPs is divided into two main types: isotropic and anisotropic. Isotropic nanomaterial is a 0-D (e.g. sphere) with the properties of a material are more or less the same regardless of directions because of the confinement of electrons to the same extent in all the three dimensions (Zhang *et al.*, 2011). Anisotropic nanomaterial usually shows direction and dimension dependent physical and chemical properties whereby tuning the properties of these particles will be difficult compared to other materials (Sajanlal *et al.*, 2011). The properties normally vary with different crystallographic orientations. Figure 2.4 shows a pictographic representation of isotropic and anisotropic nanomaterial, categorized based on the dimension.

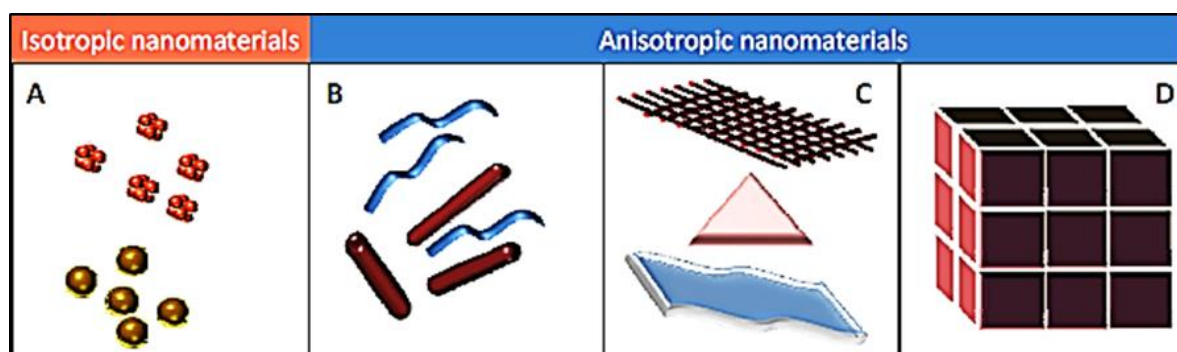


Figure 2.4: Various kinds of nanomaterials with (A) 0D spheres and clusters, (B) 1D nanofibers, wires, and rods, (C) 2D films, plates, and networks and (D) 3D nanomaterials (Sajanlal *et al.*, 2011)

AuNPs growth can take place either in a thermodynamically controlled or kinetically controlled manner (Berhault *et al.*, 2007). In the thermodynamic approach, synthesis process involves supersaturation, nucleation (homogeneous or heterogeneous), and subsequent growth. Thermodynamic growth often results in uniform growth of all crystal facets and followed by formation of spherical or near-spherical structures. In the kinetic approach, formation of nanoparticles is achieved by either limiting the amount of precursors available for the growth. The synergistic effects of both thermodynamic and the kinetic aspects play a critical role in determining nanoparticle shape. In the case of kinetically controlled growth, preferential and directional growth occurs which in turn results in the anisotropic growth (Sajanlal *et al.*, 2011).

2.2.2 Lattice parameters of AuNPs

Most solids metal is crystalline with their atoms are arranged in regular manner. Pure solid gold (Au) has an atomic number 79 with atomic weight 196.97 (Hesse, 2007). Most metals in the solid state form close-packed lattices; thus Ag, Al, Au, Co, Cu, Pb, Pt and Rh are face-centred cubic (FCC) (Poole and Owens, 2003). In FCC lattice as in Figure 2.5 shows the atoms are arranged at the corners and center of each cube face of the cell.

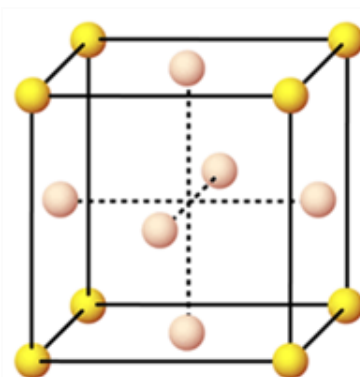


Figure 2.5: Basic structure of face centered cubic unit cell (Poole and Owens, 2003)

The relationship between the diameter of AuNPs with the total number of the atoms and the percentage of surface atoms are represented in Table 2.1. For example, when the diameter of AuNPs is 0.288 nm, the total atoms is 1 as well as surface atoms is one therefore percentage of surface atoms is 100%.

Table 2.1: The relationship between the diameter (d) of the gold particle, the total number of the atoms and the percentage of surface atoms (Poole and Owens, 2003)

Shell	Number of diameters	d, Au (nm)	Total atoms	Surface atoms	% Surface atoms
1	1d	^a 0.288	1	1	100
2	3d	0.864	13	12	92.3
3	5d	1.44	55	42	76.4
4	7d	2.01	147	92	62.6
5	9d	2.59	309	162	52.4
6	11d	3.16	561	252	44.9
7	13d	3.74	923	362	39.2
8	15d	4.32	1415	492	34.8
9	17d	4.89	2057	642	31.2
10	19d	5.47	2869	812	28.3
25	49d	14.1	4.9×10^4	5083	23.8
50	99d	28.5	4.04×10^5	2.40×10^4	5.9
100	199d	57.3	3.28×10^6	9.80×10^4	3.0

^a Diameter of gold atom is 0.288 nm.

The crystal structure of AuNPs is influenced by the type of synthesis method that has been used. For example, AuNPs synthesized using the inverse micelle technique preferentially assemble into FCC structures with long-range translational and orientation ordering while AuNPs produced using the solvated metal atom dispersion (SMAD) method predominantly form a hexagonal close-packed (HCP) nanocrystal superlattices. AuNPs synthesized using the chemical reduction process and subsequent ripening process predominantly have a faceted single crystals structure (Prasad *et al.*, 2002). Different packing behaviour are results from variation in nanoparticle core morphologies that influenced by the synthetic method. FCC

ordering is preferred by single crystalline nanoparticles, while HCP is preferred by polycrystalline nanoparticles (Stoeva *et al.*, 2003). Commonly, X-Ray Diffraction (XRD) analysis is used to characterize lattice parameter of material. High-resolution transmission electron microscopy (HRTEM) also is used to study the crystallinity of particles by observing the morphology of particles at high magnification and measure the lattice distance (d-spacing) on the atomic arrangement through microscopic measurement. In the cubic system, interplanar spacing is defined as the distance between adjacent planes (hkl) or the perpendicular distance between successive parallel planes of atoms in a crystal. Stoeva *et al.* (2003) used HRTEM, AFM and XRD to characterize the superlattice parameter and crystal structure of AuNPs synthesized using the inverse micelle method. They concluded that all these characterization methods did not show any difference when superlattice parameter as in Figure 2.6. Figure 2.6 (a) shows a perfect atomic arrangement in the particles whereby (111) atomic planes from the gold FCC lattice are clearly observed.

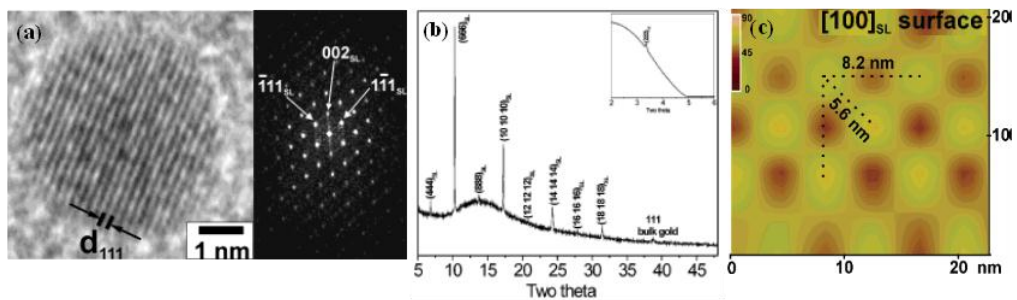


Figure 2.6: (a) HRTEM images of single crystalline AuNPs with small-angle electron diffraction (SAED) pattern, (b) XRD analysis and (c) Tapping-mode AFM images of resolved $[100]_{sl}$ superlattices surface of AuNPs synthesized by the inverse micelle method (Stoeva *et al.*, 2003)

2.2.3 Thermal properties of AuNPs

The thermal property of material such as melting point is dependent on the size of the particles (Bahadory, 2008). When the size of particles becomes smaller,

more proportion of surface atoms increases. This is due to the number of surface atoms becomes equal or even exceeds the number of inner-core atoms as particles decrease in size. In contrast, for a typical bulk material the surface is significantly small in comparison to the total volume. In crystal lattice, surface atoms are more easily rearranged than those in the centre of the particle. Thus, the melting process, which depends on destroying the order of the crystal lattice can take place a lower temperature. Consequently, as the number of atoms decreases along with the size of the AuNPs, the melting point decreasing. The melting point of gold metal is 1064°C with boiling point is 2856°C. Whereas, for 11-12 nm AuNPs it is about 1000°C, then begins to drop dramatically to 900°C for 5 to 6 nm particles and to 700°C for 2 to 3 nm particles (Klabunde Kenneth *et al.*, 2001).

AuNPs are also affected by the presence of thermal energy after synthesis. Magnusson *et al.* (1999) studied “reshaping” treatment of the AuNPs (20 nm range) produced using evaporation in a high-temperature tube furnace and subsequent size selection. They found that in order to obtain spherical particles, it is necessary to reshape the particles at high temperature, which was investigated for temperatures between 25°C and 1200°C (Magnusson *et al.*, 1999). HRTEM analysis showed that the degree of crystallinity became higher with increasing reshaping temperature (Figure 2.7). Untreated particles (Figure 2.7a) had an irregular shape, but at temperature 200°C the gold particles already became compact and nearly spherical (Figure 2.87). Even at 745°C (Figure 2.7c), the compact particles were still polycrystalline. At 1170°C the particles melted and became almost single crystalline (Figure 2.7d), although they might still comprises of defects. At this time the particle

was faceted. Although it contained a defect, some crystalline order seemed to prolong over the entire particle since the facets are symmetry.

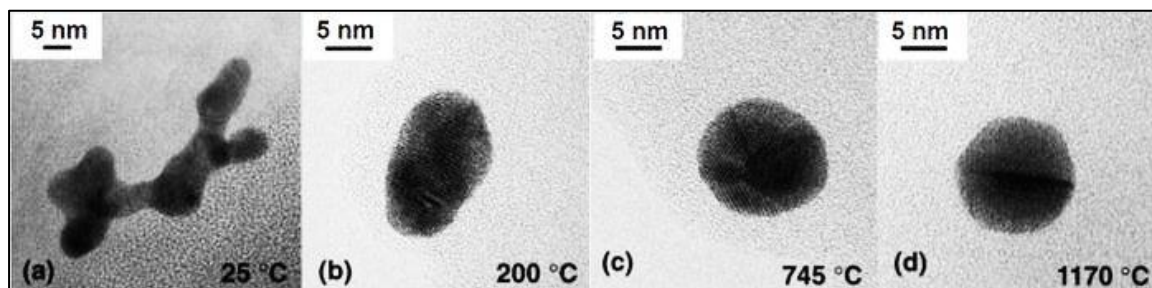


Figure 2.7: TEM images of AuNPs reshaped at different temperatures (Magnusson *et al.*, 1999)

2.2.4 Optical properties of AuNPs

The optical properties of metal nanoparticles have gained attention in physical chemistry since middle 1800s (Kelly *et al.*, 2002). AuNPs have an extraordinarily high extinction coefficient originating from the inherent plasmonic properties (Storhoff *et al.*, 2000). Their optical properties are strongly dependent on the interparticle separation distance and aggregation that cause a massive shift in the extinction spectrum manifested as a color change of suspensions from red to purple (Faraday, 1857). Most AuNPs-based colorimetric sensors are designed in such a way that binding of an analyte causes particle aggregation and consequently produce a colorimetric response (Stewart *et al.*, 2008).

An example of the interaction between light and electrons of AuNPs is represented in Figure 2.8. The oscillating electric field causes the conduction electrons to oscillate coherently when a small spherical metallic nanoparticle is irradiated by a light. In order for this phenomenon to take place, the particle must be much smaller than the wavelength of incident light. The electric field of incident

light can induce an electric dipole in the metal particle by displacing many of the delocalized electrons in one direction away from the rest of the metal particle and consequently generating a net negative charge on one side. As a result, a net positive charge presence in the opposite side on the nuclei. The collective oscillation of electrons is called the dipole plasmon resonance to differentiate from plasmon excitation that can occur in bulk metal or metal surfaces. Under these circumstances, the electric field of the light can be considered as constant, and the interaction is governed by electrostatics rather than electrodynamics (Kelly *et al.*, 2002).

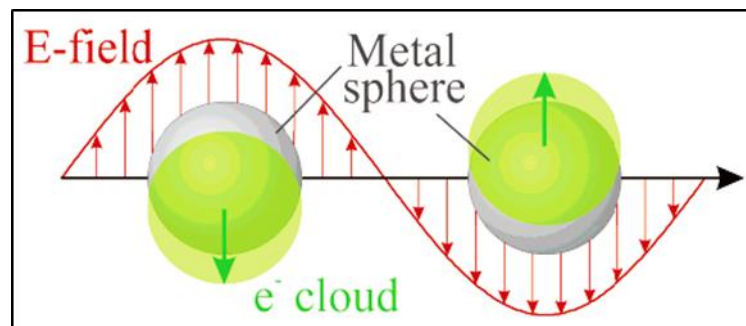


Figure 2.8: Schematic of plasmon oscillation for a sphere, showing the displacement of the conduction electron charge cloud relative to the nuclei (Kelly *et al.*, 2002)

Mie first described this phenomenon theoretically by solving Maxwell's equations for a radiation field interaction with a spherical metal particle under the appropriate boundary conditions that determine its position, intensity and broadness (Kelly *et al.*, 2002). The only material-related functions and constants in Mie's theory are the complex dielectric function of the metal and the dielectric constant of the surrounding medium (Link *et al.*, 1999). The absorption band, which is induced by an electromagnetic field, is referred to as the "surface plasmon resonance (SPR)". The surface plasmon appears in the absorption spectrum due to the collective coherent oscillation of the conduction band electrons occupying energy states just

above the Fermi level. The position of the surface plasmon depends on several factors among which particle size and shape as well as nature of the surrounding (Alvarez *et al.*, 1997, Kreibig and Genzel, 1985, Norman *et al.*, 2002, Persson, 1993). The surrounding medium is often referred as the capping material that is important to prevent aggregation followed by precipitation of Au and other metal particles in solution (Link *et al.*, 1999).

Bohren (1983) found that AuNPs in spherical shape shows a strong absorption band in the visible region of the electromagnetic field at about 520 nm. This absorption, term as plasmon absorption is absent for very small particles (≤ 2 nm) as well as for bulk gold (Bohren, 1983). The plasmon absorption originates from the oscillation of the free electrons (6s-electrons of the conduction band in the case of gold). Link and El-Sayed (2000) studied the effect of the SPR for spherical Au colloids with varying diameters as shown in Figure 2.9.

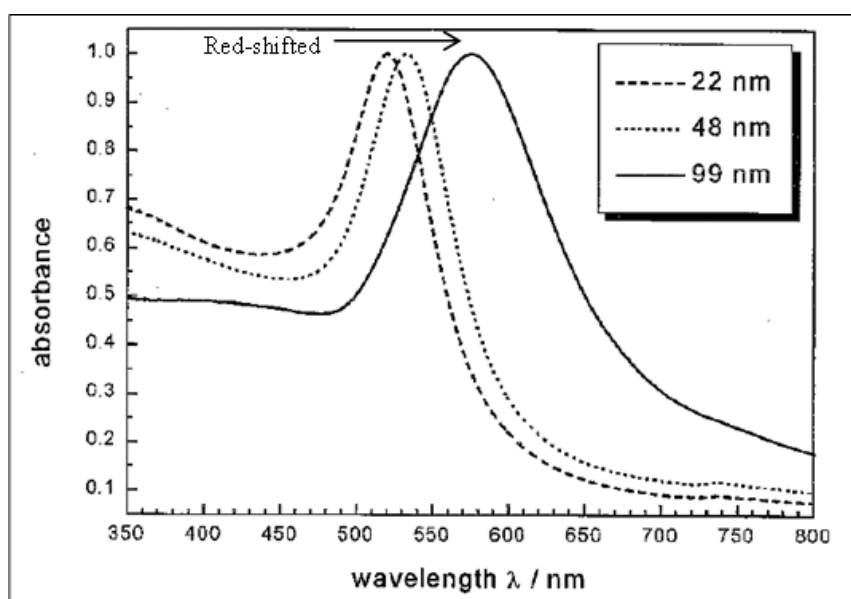


Figure 2.9: SPR of 22 nm, 48 nm and 99 nm spherical AuNPs (Link and El-Sayed, 2000)

As the particle size of AuNPs increases, the plasmon band frequency decreases or shifts to longer wavelengths (red-shifted). They suggested that in small particles such as AuNPs with diameter less than 20 nm, extinction of light is primarily due to absorption. Larger particles tend to demonstrate much stronger scattering (Link and El-Sayed, 2000).

2.2.5 Steric stabilization and electrostatic properties of AuNPs

Nanoparticles are stable in colloidal form or solution due to the electrostatics repulsion of their surface charge. Insufficient surface charge or stabilizing agent causes the particles to aggregate or precipitate (Khan, 2008, Turkevich *et al.*, 1951). The use of stable nanoparticle dispersions is often required to correlate nanoparticle physicochemical properties with their toxic potential. A general criterion to prepare stable dispersion is to increase repulsive forces between particles such that agglomeration is suppressed or is kinetically slow.

Jiang *et al.* (2009) demonstrated electrostatic stabilization by adjusting pH of AuNPs to increase particle surface charge in order to increase the repulsive force between particles. If a particle is ionic or has highly polar bonds, multiply charged ions may be adsorbed by the particle in aqueous environment leading to an increase in particle surface charge and zeta potential (Jiang *et al.*, 2009). In the absence of suitable stabilizing agents, colloidal particles are attracted to each other by van der Waals forces that results in the coagulation and precipitation of the sol due to the repulsion barrier between the approaching particles (Figure 2.10a). There are two methods for stabilization, electrostatic and steric. Electrostatic stabilization involves the use of charged capping agents such as sodium citrate (Li *et al.*, 1999). Steric

stabilization of colloidal particles is achieved by attaching (grafting or chemisorption) macromolecules commonly polymeric molecules to the surfaces of the particles (Fritz *et al.*, 2002).

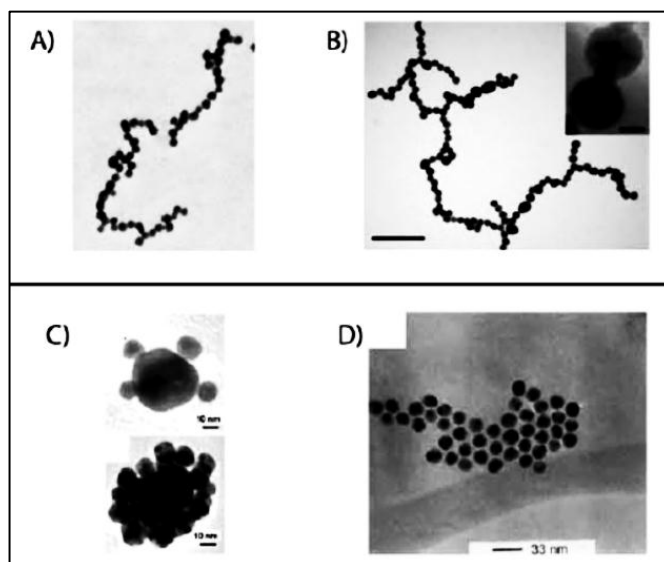


Figure 2.10: AuNPs interaction and assembly with (A – B): Linear assembly driven by van der Waals forces and electrostatic interactions while (C – D) demonstrated the specific interaction between chemical moieties (Shaw *et al.*, 2011)

For AuNPs reduced using sodium citrate, citrate ions adsorbed onto the particle's surface creating a surface charge that stabilizes the particles (Turkevich *et al.*, 1951). Citrate capped nanoparticles are negatively charged and attract positively charged counter-cations from the solution which results in the formation of a diffuse electrical double layer and consequently a Coulombic repulsion occurs between the particles (Figure 2.11). As long as the electric potential associated with the double layer is high, electrostatic repulsion between the particles will prevent agglomeration. In addition, changes in temperature may cause a sensitive double layer and amend the ionic strength of the solution. The ionic strength could be increased by the addition of salt that compress the double layer and shorten the range

of repulsion. Charge reduction on the colloid AuNPs by the addition of a neutral strongly binding and displace the absorbed citrate anions and would result in agglomeration (Jerez-Rozo, 2007).

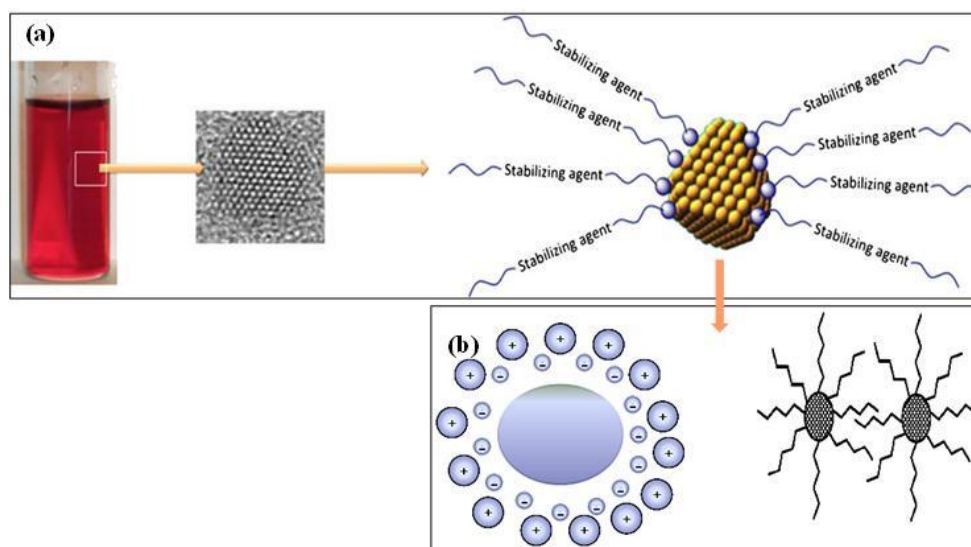


Figure 2.11: (a) General schematic representation of the stabilization forces in colloidal AuNPs (b) after citrate reduction (Jerez-Rozo, 2007)

2.2.6 Biological properties of AuNPs

Nanomaterials, especially AuNPs including spherical particles, nanorods, and nanoshells with a size ranging from 10 to 100 nanometers are well known to have unique physico-chemical properties such as ultra-small size, large surface area to mass ratio, high surface reactivity, biocompatibility, ease of surface functionalization and have a large light absorption (Liu *et al.*, 2008, Patra *et al.*, 2009). The magnitude of light scattering by AuNPs can be in orders of magnitude higher than light emission from strong fluorescence dyes (Link and El-Sayed, 1999b, Nikoobakht and El-Sayed, 2003, Sun and Xia, 2002). These unique properties of AuNPs enable it to be a promising material in the biomedical field such as molecular and cell imaging,

biosensing, bioassays and photothermal therapy (El-Sayed *et al.*, 2005, Huang *et al.*, 2006, Katz *et al.*, 2004).

The biological properties such as cytotoxicity, immunogenicity and biocompatibility of AuNPs are correlated directly when using different physico-chemical techniques (Shukla *et al.*, 2005). Cytotoxicity is the feature of existence toxic to the cell. Shukla *et al.* (2005) have concluded that Au (0) nanoparticles are not cytotoxic, reduced the production of reactive oxygen and nitrite species, and do not cause secretion of proinflammatory cytokines. These features made AuNPs a suitable candidate for nanomedicine. Likewise, Pan *et al.* (2007) proved that the cytotoxicity of triphenylphosphine monosulfonate (TPPMS) / tris-sulfonated triphenylphosphine (TPPTS) modified AuNPs depend predominantly on their size and not on ligand chemistry (Pan *et al.*, 2007). They observed that AuNPs of 1–2 nm in size were highly toxic and both smaller gold compounds and larger 15 nm AuNPs were reasonably nontoxic.

Fan *et al.* (2008) reported the effects of AuNPs with different sizes on biocompatibility of water-soluble and concentrations to human bone marrow mesenchymal stem cells (hBMSCs) and human hepatoma carcinoma cells (HuH-7). In their observation, more than 80% cell survival when both cells were incubated with 71.1 µg/ml of 15 and 30 nm AuNPs (Fan *et al.*, 2008). In addition, AuNPs are exceptionally stable against oxidation and therefore play an important role in the advancement of clinically useful diagnostic and therapeutic nanomedicines (Hainfeld *et al.*, 2006, Murphy *et al.*, 2008, Pan *et al.*, 2007). Connor *et al.* (2005) have examined the uptake and potential toxicity of 18 nm of naked AuNPs and with

surface modifier in human leukemia cells for 3 days exposure. The surface modifiers of AuNPs incorporated a range of anionic (e.g. citrate), neutral (e.g. cysteine, glucose and biotin) and cationic clusters (cetyltrimethylammonium bromide; CTAB). The data in Figure 2.12 suggested that none of the spherical AuNPs were toxic to the human leukemia cells up to 100 μM in gold atom concentration, even though they were being taken up into the cells (confirmed by TEM images of cell slices).

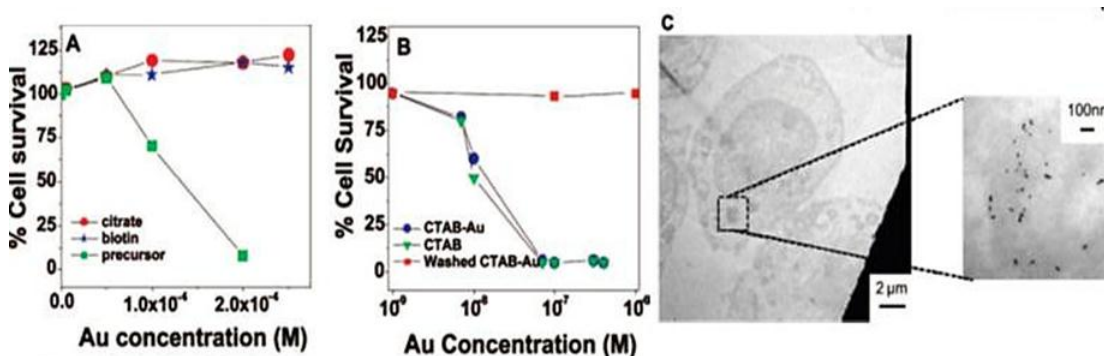


Figure 2.12: Cell survival data upon exposure to AuNPs for 3 days; cell viability measured by Microculture Tetrazolium (MTT) assay: (A) survival of cells exposed to 18 nm AuNPs (citrate-capped); (B) survival of cells exposed to 18 nm AuNPs (CTAB capped); (C) TEM images show the cells with AuNPs with inset the high magnification image of a small region in the cell cytoplasm containing AuNPs (Connor *et al.*, 2005)

However, most works found that the nanoparticle precursors; CTAB and the gold salt; HAuCl_4 , were toxic to the cells at 10 nM (Nikoobakht and El-Sayed, 2001, Sau and Murphy, 2005). This is due to free CTAB (which may result from unfinished purification of the gold nanorods or desorption from the bound bilayer) could cause toxic to cells because it is a detergent that can break open cell membranes. Hence, the appropriate purification of the gold particles (rods, spheres) is a key step for any *in vivo* work (Murphy *et al.*, 2008).